Available online at www.sciencedirect.com
ScienceDirect
Polymer 49 (2008) 1312–1322
polymer
www.elsevier.com/locate/polymer

The role of organoclay in promoting co-continuous morphology in high-density poly(ethylene)/poly(amide) 6 blends

G. Filippone [a,*], N.Tz. Dintcheva [b], D. Acierno [a], F.P. La Mantia [b]

[a] Dipartimento di Ingegneria dei Materiali e della Produzione, Università di Napoli Federico II, Piazzale V. Tecchio 80, 80125 Napoli, Italy
[b] Dipartimento di Ingegneria Chimica dei Processi e dei Materiali, Università di Palermo, Viale delle Scienze, Ed. 6, 90128 Palermo, Italy

Received 19 November 2007; received in revised form 11 January 2008; accepted 14 January 2008
Available online 26 January 2008

Abstract

The effect of organically modified clay on the morphology, rheology and mechanical properties of high-density polyethylene (HDPE) and polyamide 6 (PA6) blends (HDPE/PA6 = 75/25 parts) is studied. Virgin and filled blends were prepared by melt compounding the constituents using a twin-screw extruder. The influence of the organoclay on the morphology of the hybrid was deeply investigated by means of wide-angle X-ray diffractometry, transmission and scanning electron microscopies and quantitative extraction experiments. It has been found that the organoclay exclusively places inside the more hydrophilic polyamide phase during the melt compounding. The extrusion process promotes the formation of highly elongated and separated organoclay-rich PA6 domains. Despite its low volume fraction, the filled minor phase eventually merges once the extruded pellets are melted again, giving rise to a co-continuous microstructure. Remarkably, such a morphology persists for long time in the melt state. A possible compatibilizing action related to the organoclay has been investigated by comparing the morphology of the hybrid blend with that of a blend compatibilized using an ethylene–acrylic acid (EAA) copolymer as a compatibilizer precursor. The former remains phase separated, indicating that the filler does not promote the enhancement of the interfacial adhesion. The macroscopic properties of the hybrid blend were interpreted in the light of its morphology. The melt state dynamics of the materials were probed by means of linear viscoelastic measurements. Many peculiar rheological features of polymer-layered silicate nanocomposites based on single polymer matrix were detected for the hybrid blend. The results have been interpreted proposing the existence of two distinct populations of dynamical species: HDPE not interacting with the filler, and a slower species, constituted by the organoclay-rich polyamide phase, which slackened dynamics stabilize the morphology in the melt state. In the solid state, both the reinforcement effect of the filler and the co-continuous microstructure promote the enhancement of the tensile modulus. Our results demonstrate that adding nanoparticles to polymer blends allows tailoring the final properties of the hybrid, potentially leading to high-performance materials which combine the advantages of polymer blends and the merits of polymer nanocomposites.

Keywords: Nanocomposite polymer blend; Morphology; Co-continuity

1. Introduction

Polymer blending has gained much interest as a suitable way to tailor the properties of polymeric materials without investing in new chemistry. Polymer blends represent a large and rapidly growing fraction of all plastics produced. The opportune choice of the blend constituents and the control of microstructure can lead to multiphase systems with enhanced performances [1–3]. Besides mixing polymeric components, it is more than 50 years that filling polymers with inorganic particles receives industrial and scientific consideration because it offers an economical method to produce new materials with enhanced properties compared with neat polymers. When the characteristic filler sizes are in the nanometer scale, polymer-nanocomposite systems are formed. Polymer-layered silicate nanocomposites represent a radical alternative to conventionally filled polymers.

* Corresponding author. Tel.: +39 081 7682407; fax: +39 081 7682404.
E-mail address: gfilippo@unina.it (G. Filippone).

0032-3861/$ - see front matter © 2008 Elsevier Ltd. All rights reserved.
doi:10.1016/j.polymer.2008.01.045

Since the early 1990s, when Toyota researchers synthesized a montmorillonite/nylon 6 hybrid [4], the possibility of industrially exploiting the capacity of clays to be dispersed in a polymer matrix has been extensively investigated owing to the outstanding properties potentially achievable also for very low filler contents [5–10].

In the light of the previous remarks, nanocomposites based on multicomponent polymer systems could represent a promising way to produce new materials with high performance. Nevertheless, the literature concerning polymer blends/clay systems is still lacking. This is not surprising, considering that the morphology of hybrid polymer blends, playing a key role in determining their final properties, arises from complex physical and chemical interactions occurring between the phases on both nano- and microscale. This makes challenging any general description of the properties of nanocomposite polymer blends, and most of the results recently reported in the literature on this subject [11–15] should be circumscribed to the specific systems considered.

The objective of the present study is focused on the analysis of the relationships between morphology and technologically relevant properties, such as rheological and mechanical properties, of a nanocomposite polymer blend constituted by high-density polyethylene and polyamide 6 (HDPE/PA6 = 75/25 parts) filled with small amounts (5 parts) of an organomodified montmorillonite. HDPE/PA6 blends are already employed in a variety of packaging and automotive products, and the addition of nanoreinforcements could results in improved performances. The first part of the work is devoted to the analysis of the materials' morphology on both nano- and microscale. This represents an indispensable requisite to correctly interpret the macroscopic behaviour of the studied systems. A wide variety of investigation techniques have been employed: wide-angle X-ray diffractometry (WAXD) and transmission electron microscopy (TEM) were used to detect the state of dispersion of the clay platelets on nanoscale; scanning electron microscopy (SEM), in combination with selective extraction experiments, differential scanning calorimetry (DSC) and thermogravimetrical analyses (TGA), allowed identifying the micron-scale arrangement of the polymer phases. A possible compatibilizing action related to the organoclay is discussed by using a reference blend prepared using an ethylene–acrylic acid copolymer as a compatibilizer precursor. Linear viscoelastic rheology is employed to probe into the melt state dynamics of the samples, and tensile properties are discussed in the light of the knowledge of the blends' morphology.

2. Experimental

2.1. Materials and blend preparation

The polymeric constituents of the samples are a high-density polyethylene (HDPE, Eraclene® MP94 from *Polimeri Europa*, Italy), with density $\rho = 0.96$ g/cm^3 at 23 °C and $MFI_{190\ ^\circ C/2.16\ kg}$ of 7.0 g/10′, and a polyamide 6 (PA6, Radilon® S from Radici Group, Italy), with $\rho = 1.13$ g/cm^3 and intrinsic viscosity of 1.5 dL/g measured at 30 °C in 80 vol% formic acid. A compatibilizer precursor based on an ethylene–acrylic acid copolymer (EAA, Escor® 5001 from Exxon-Mobil Chemical Mediterranea) was employed to prepare a compatibilized blend. It has an acrylic acid content of 2.5 mol%, $MFI_{190\ ^\circ C/2.16\ kg}$ of 2.0 g/10′ and $\rho = 0.931$ g/cm^3. An organomodified clay (Cloisite® 15A from Southern Clay Products) was used to prepare the hybrid blend. Cloisite® 15A is a montmorillonite modified by dimethyl-dihydrogenated tallow-quaternary ammonium cation with concentration of the organomodifier of 125 mequiv/100 g clay and density $\rho = 1.66$ g/cm^3.

The constituents were melt-compounded in a co-rotating intermeshing twin-screw extruder (OMC, Italy). A cylindrical capillary die was used (diameter 1.5 mm, length 15 mm), and the extrudate was cooled in water at the die exit, dried by air and then granulated. The thermal profile was 140–200–240–240–240–220 °C and the screw speed was set to ~60 rpm, corresponding to residence times in the order of ~150 s. The neat polymers used as reference materials were extruded in the same conditions. PA6, the organoclay and EAA were dried under vacuum for 12 h before the extrusions. The drying temperatures were 90 °C for polyamide and Cloisite® 15A, and 70° for EAA. The designations and compositions of the samples are reported in Table 1.

2.2. Characterization methods

Wide-angle X-ray diffractometry (WAXD) was performed at room temperature in the reflection mode on a Siemens D-500 X-ray diffractometer with Cu Kα radiation of wavelength of 1.54 Å. A scanning rate of 10°/min was used. The nanostructure of the hybrid blend was observed by means of transmission electron microscopy (TEM) using a Philips EM 208 TEM with 100 keV accelerating voltage. The specimens were thin layers (thickness ~150 nm) microtomed from the extruded pellets using a diamond knife at room temperature.

Soxhlet extraction experiments were performed in order to separate the polymer phases of the sample HDPE/PA6/clay using boiling toluene, which is a good solvent for HDPE and a non-solvent for polyamide. The extraction process, carried out upon several pellets as extruded, was protracted for two weeks. Before the subsequent analyses, the extracted and non-extracted samples were dried for 48 h at 90 °C under vacuum to purge the solvent.

Differential scanning calorimetry (DSC) was performed using a TA Instruments Q1000 DSC. In order to erase any thermal history effect, the samples were heated from 20 °C to 300 °C, cooled to 20 °C, and then they were heated again up to 300 °C. The data presented refer to the second heating scans. The heating and cooling cycles were all carried out at 10 °C min^{-1} under nitrogen atmosphere. A TA Instrument Q5000 TGA was used for the thermogravimetric analyses (TGA). The samples were

Table 1
Designations and compositions of the samples

Sample	Designator	Parts
HDPE/PA6	HDPE/PA6	75/25
HDPE/PA6/Cloisite® 15A	HDPE/PA6/clay	75/25/5
HDPE/PA6/Escor® 5001	HDPE/PA6/EAA	75/25/5
HDPE/Cloisite® 15A	HDPE/clay	100/5
PA6/Cloisite® 15A	PA6/clay	100/5

heated from 30 °C to 800 °C at 10 °C min^{-1} under nitrogen atmosphere, and the residuals at 800 °C were evaluated.

Rheological tests were performed using a strain-controlled rotational rheometer in parallel plates geometry with either 25 mm or 50 mm diameter plates. All measurements were carried out at 240 °C in nitrogen atmosphere. The pellets as extruded were loaded between the plates of the rheometer and compressed using a containment ring in order to obtain disks (thickness ~2 mm) suitable for rheological analyses. The duration of this procedure was ~300 s. Once removed the ring and cleaned the excess material, the tests were started.

Preliminary linearity check tests were carried out in order to detect the linearity limits of the samples. Time sweep experiments allowed investigating the temporal stability of the viscoelastic properties. In order to contain as much as possible the experimental times, multiwave tests were performed to get the linear frequency-dependent elastic (G') and viscous (G'') moduli. In a multiwave test the sample is subjected to a strain waveform, $\gamma(t)$, constituted by the sum of the Fourier series described by a sinusoidal strain at a fundamental frequency, ω_f, and seven sinusoidal strains, each at a harmonic frequency of the fundamental, $\gamma(t) = \sum_i \gamma_i \sin(n_i \omega_f t)$. We set $\omega_f = 0.1$ rad/s, $n_i = 1, 2, 6, 10, 20, 60, 100$, and 200, while the strain amplitudes, γ_i, were opportunely chosen for each sample according to the requirement that $\sum \gamma_i$ must stay below the linear viscoelastic limit previously evaluated. From the stress response, the individual stresses at each frequency, thus $G'(\omega)$ and $G''(\omega)$, were obtained by means of a discrete Fourier transformation. Quick frequency scans from $\omega = 10^1$ rad/s to $\omega = 10^2$ rad/s were performed to extend the results of multiwave tests to higher frequencies, while longer dynamics were probed by means of stress relaxation measurements in linear regime.

A scanning electron microscope SEM Leica 420 was employed to inspect the cryo-fractured surfaces of samples recovered immediately before starting rheological tests. Teflon sheets were used to facilitate the removal of the samples from the plates of the rheometer. SEM observations were carried out also upon the powder remaining after the Soxhlet extraction of the sample HDPE/PA6/clay. The fracture surfaces and the powders were coated with gold before the investigations.

Quantitative extraction experiments were performed in order to check the degree of co-continuity, φ, of the blends. Several disks (diameter 25 mm, thickness ~2 mm) of the samples HDPE/PA6 and HDPE/PA6/clay, recovered at the beginning of rheological tests, were immersed in formic acid for five days. Once removed from solution, the samples, all remaining self-supporting, were dried under vacuum at 90 °C for 48 h and their mass was evaluated. The procedure was repeated until a constant sample mass was attained, typically three times. Since formic acid is a good solvent for PA6 and a non-solvent for HDPE, the change in weight during extraction and the knowledge of the nominal composition of the samples lead to the estimation of φ as $\varphi = (m_0 - m_f)/m_0$, where m_0 and m_f represent, respectively, the mass of PA6 present in the blend before and after the extraction process [16,17].

Tensile properties were determined at room temperature and humidity using an Instron machine mod. 4443 according to ASTM test method D882. The specimens were cut from compression-molded sheets prepared using a laboratory Carver press. After keeping the materials at 240 °C for about 3 min, the plates of the press were cooled at room temperature with a water-cooling system. The samples, stored for one week at room temperature and humidity, were tested at 1 mm/min up to a strain of 10%, and then the speed was increased up to 50 mm/min until break. The Young's modulus, tensile strength and elongation at break were recorded. The data reported are the average values obtained by analyzing the results of eight tests per sample and the reproducibility was found to be ±8%.

3. Results and discussion

3.1. Analysis of the morphology on nanoscale

3.1.1. Wide-angle X-ray diffractometry

Wide-angle X-ray diffractometry was used in order to investigate the state of dispersion of the organoclay within the hybrid samples. The angular dependences of the scattering intensities are shown in Fig. 1a for Cloisite® 15A and various hybrids with five parts of organoclay and different polymer matrices. WAXD is based upon the interference pattern produced by repetitive structures in the organoclay. The low-angle peaks correspond to the {001} basal reflection of the montmorillonite aluminosilicate. From the angular location of the peaks and the Bragg's condition the interlayer spacing, d_{001}, of each sample was determined. The computed values are summarized in Fig. 1b. The pristine organoclay exhibits a peak at $2\theta = 2.81°$, corresponding to $d_{001} = 3.14$ nm. Dispersing Cloisite® 15A in PA6 is not easy and specific melt processing conditions are

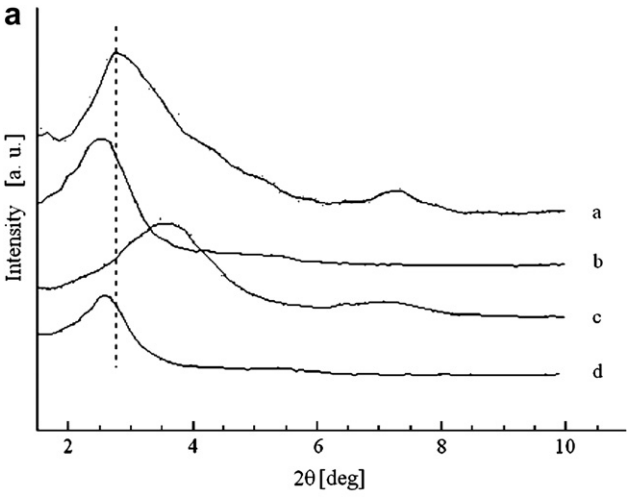

b

Sample	Material(s)	d_{001} (nm)
a	Cloisite® 15A (Clay)	3.14
b	PA6/Clay	3.43
c	HDPE/Clay	2.40
d	HDPE/PA6/Clay	3.21

Fig. 1. (a) WAXD patterns and (b) interlayer distances, d_{001}, for Cloisite® 15A and various hybrids with 5 phr of organoclay and different polymer matrices.

required to get delaminated the organoclay stacks [18]. The WAXD pattern of the hybrid PA6/clay, however, indicates a slight increase of the interlayer distance due to the insertion of small amounts of PA6 chains between the silicate layers. Conversely, a clear decrease of d_{001} occurs for the sample HDPE/clay. The organoclay modifying alkyl ammonium groups of Cloisite® 15A degrade quite rapidly in the temperature range of 200–300 °C [19]. Since the processing conditions used to melt compound the studied materials fall in this range, the collapsed structure of the sample HDPE/clay could be due to the thermo-degradation of the organomodifier and the consequent dissolution of the degradation products, predominantly constituted by α-olefins, into the polyethylene matrix [20]. The sample HDPE/PA6/clay exhibits a small increase of d_{001} with respect to the pristine organoclay. Since HDPE is the predominant phase of the hybrid blend, such a result is surprising if compared with the clear reduction of the interlayer distance detected for the sample HDPE/clay. Recent results by Chow et al. show that the organomodified clay exclusively locates inside the major polyamide phase in uncompatibilized polyamide 6/polypropylene blends [21,22]. Thus, the WAXD results shown in Fig. 1 may be explained by considering that the organoclay preferentially locates into the more hydrophilic PA6 phase, so that its collapse would be prevented due to the small solubility of the α-olefins into polyamide. On the other hand, the negligible degree of intercalation could be a consequence of a poor stress transfer between the two polymer phases during the melt compounding.

3.1.2. Transmission electron microscopy

The previous conjectures about a preferential location of the clay within the PA6 phase of the hybrid blend need to be critically tested by means of further morphological analyses. Transmission electron microscopy was employed to inspect the nanostructure of the sample HDPE/PA6/clay. TEM investigations are based upon electron density and diffraction contrast differences between the clay structures and the polymeric suspending medium. Three TEM micrographs of a randomly microtomed extruded pellet of the sample HDPE/PA6/clay are shown in Fig. 2. A complex morphology can be noticed on both micro- and nanoscale. Organoclays in a polymer matrix appear as dark features, so that the micron-sized items detectable in Fig. 2a should contain high amounts of silicate layers. The magnifications of one of these domains shown in Fig. 2b and c confirm such statement, and agglomerated organoclay stacks with thickness of few tens of nanometers are observable. In agreement with the WAXD analyses, however, neither exfoliated nor intercalated nanostructures can be clearly recognized.

The relevant non-homogeneity detected on microscale indicates that the filler is predominantly confined into well-defined micron-sized volumes. Recently, Feng et al. have studied the morphology of blends of polypropylene and polyamide 6/clay nanocomposites [23]. Their TEM investigations, supported by energy dispersive X-ray (EDX) experiments, show that the clay preferentially locates at the interface between the polymer phases. As a consequence, the nanocomposite PA6 phase appears clearly discernable in the TEM micrographs as globular droplets with dark edges. Similarly, the inclusions shown in Fig. 2a exhibit well-defined boundaries, suggesting that they could be constituted by an organoclay-rich PA6 phase surrounded by the organoclay-poor HDPE matrix. In addition, this appears in agreement with the hypotheses emerged from the WAXD analyses. In our case, however, the absence of shadings in the inclusions does not indicate a preferential location of the organoclay in the interphase region.

3.2. Thermal analyses

3.2.1. Differential scanning calorimetry

In order to validate the hypotheses emerged from WAXD and TEM analyses about the preferential location of the organoclay into the polyamide phase of the hybrid blend, the sample HDPE/PA6/clay was subjected to a Soxhlet extraction with boiling toluene, which is a good solvent for HDPE and a non-solvent for PA6. Then, the extracted and non-extracted samples were subjected to differential scanning calorimetry and thermogravimetrical analyses. The DSC traces of the second heating scans are shown in Fig. 3 for different samples, and the temperatures, T_m, and the enthalpies, ΔH_m, of the melting peaks are summarized in Table 2. The crystalline structure of PA6 may involve different crystalline forms, coexisting in different amount depending on the cooling rate. Usually, PA6 crystallizes into the monoclinic α-form ($T_{m(\alpha)} \sim 220$ °C). The second stable

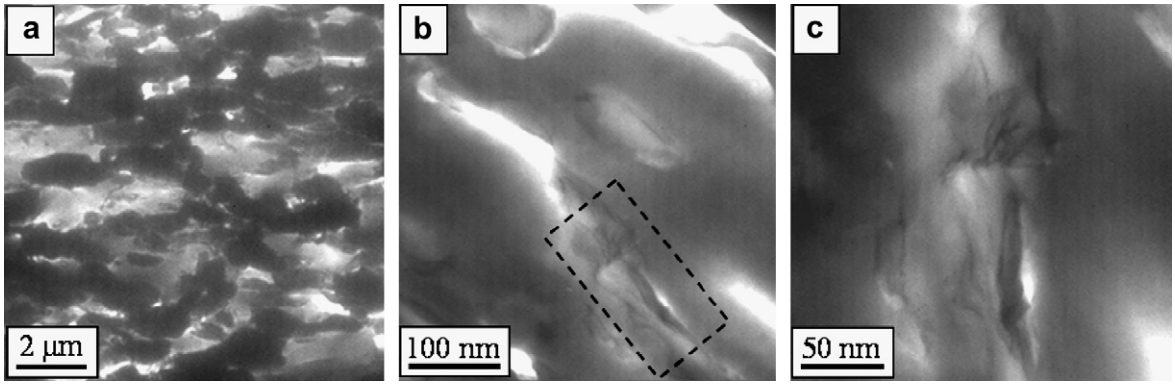

Fig. 2. (a–c) TEM micrographs of the sample HDPE/PA6/clay at increasing magnifications. The micrograph (c) is the enlargement of the nanostructure in the selected zone of (b).

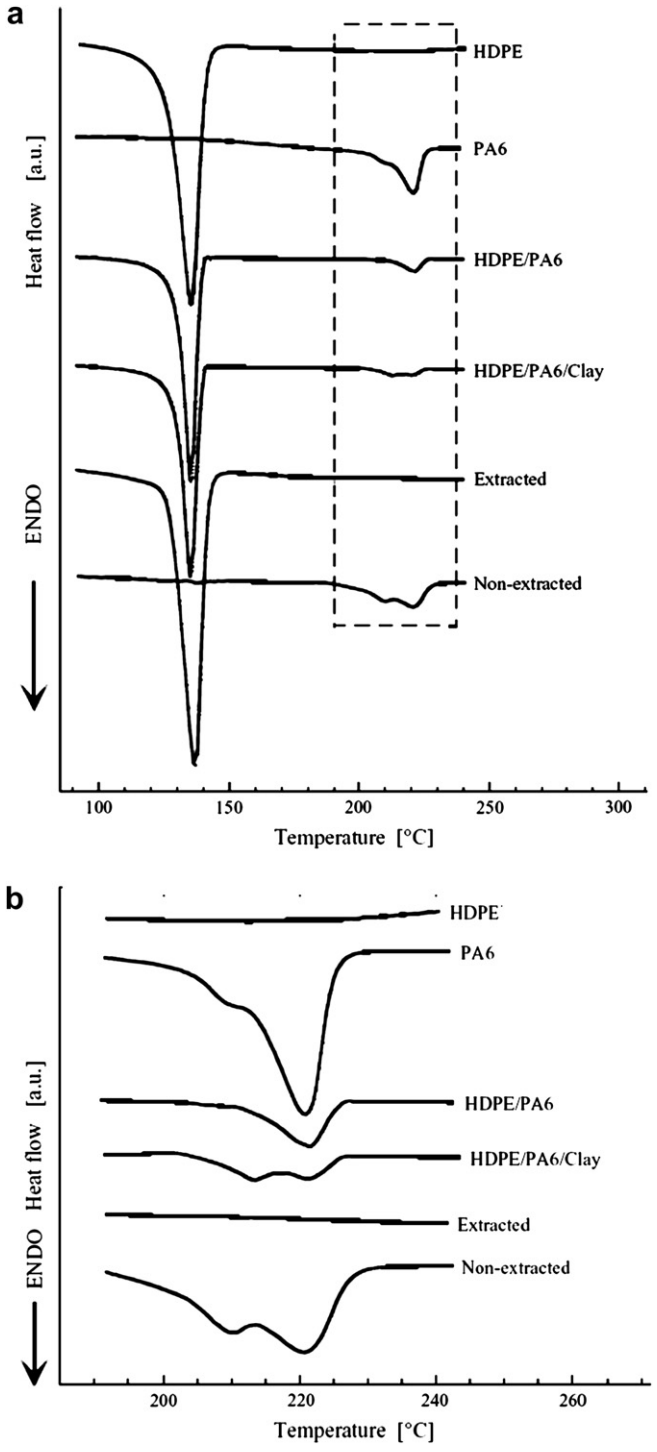

Fig. 3. (a) DSC traces of the second heating scans for different samples. The enlargement of the selected zone of (a) is shown in (b).

crystalline structure of PA6 is the γ-form ($T_{m(\gamma)} \sim 210$ °C), appearance of which is not unusual in samples cooled after mechanical blending [24]. The neat PA6 used in this work shows a predominant α-peak at ~221 °C and a shoulder at ~210 °C indicative of the coexistence of both α- and γ-form; HDPE exhibits a distinct melting peak at ~135 °C. Blending the two polymers does not affect the melting temperatures of the constituents remarkably and the melting enthalpies quite well reflect the

Table 2
Temperatures, T_m, and enthalpies, ΔH_m, of the melting peaks of the second DSC heating scans for various samples

Sample	HDPE melting peak		PA6 melting peak(s)		
	T_m (°C)	ΔH_m (J/g)	$T_{m(\alpha)}$ (°C)	$T_{m(\gamma)}$ (°C)	$\Delta H_{m(\alpha+\gamma)}$ (J/g)
HDPE	135	169.6			
PA6			221[a]	210[a]	31
HDPE/PA6	135	105.1	221	–	6.9
HDPE/PA6/clay	135	104.1	222	214	5.7
Extracted	135	174.3	–	–	–
Non-extracted	137	0.3	221	210	29.6

[a] Shoulder.

blend composition. The comparison between the DSC traces of the samples HDPE/PA6/clay and HDPE/PA6 allows evaluating the effect of the organoclay on the crystalline structures of the two polymer phases. The melting temperature of the polyethylene is unaffected by the presence of the filler and only a negligible percentage reduction of the melting enthalpy was observed. This is not unprecedented, as Cloisite® 15A has been shown to not influence the crystalline fraction of HDPE remarkably [13]. A reduced melting enthalpy and the appearance of a distinct melting peak at around 214 °C characterize the polyamide phase in the hybrid blend. The detection of the crystalline structures of polymer samples would require a detailed microstructural characterization that is beyond the scopes of this work. We observe, however, that the additional peak could reflect an increase of the γ crystalline fraction for PA6. The presence of clay in the molten PA6 has been shown to lead to a crystalline structure with considerable fractions of γ-form; moreover, a slight reduction of the crystalline content has been reported in PA6/clay hybrid samples [25–27]. Thus, in agreement with the hypotheses previously emerged from the analysis of the WAXD patterns and TEM micrographs, the data shown in Fig. 3 and Table 2 are compatible with the presence of organoclay within the minor polyamide phase of the hybrid blend. Nothing can be said, however, about the location of the filler in the polyethylene phase. The analysis of the melting peaks of the extracted and non-extracted samples confirms the efficiency of the Soxhlet extraction in separating the polymer phases: the absence of endothermic peaks in the temperature range for the melting of PA6 can be noticed for the extracted sample dissolved in toluene, indicating that its polymer fraction is constituted by neat HDPE; conversely, the melting of the polymer fraction not soluble in toluene mainly occurs between 190 °C and 230 °C, and only a negligible peak at around 137 °C can be observed. This means that the non-extractable phase is almost solely constituted by PA6. Furthermore, as previously discussed, the distinct melting peak at ~210 °C may suggest the presence of the organoclay within this polyamide-based non-extracted sample.

3.2.2. Thermogravimetrical analyses

Once separated and recognized, the extracted and non-extracted samples were subjected to TGA analyses in order to quantify the actual amounts of filler inside the two polymer phases. The residuals at 800 °C are given in Table 3 for the neat organoclay, the HDPE/PA6/clay blend and the

Table 3
Results of TGA analyses for various samples

Sample	Residual at 800 °C (wt%)
Clay	56.5
HDPE/PA6/clay	3.1
Extracted	0.6
Non-extracted	11.2

polyethylene- and polyamide-based samples recovered after the Soxhlet extraction in boiling toluene. A weight loss of 43.5% occurs for the pristine organoclay as a consequence of the thermo-degradation of the organomodifier. Thus, a residual of ~2.8% is expected for the nanocomposite blend on the basis of its nominal composition, in reasonable agreement with the value of 3.1% experimentally found. The comparison of the residuals of the extracted and non-extracted samples clearly indicates that the organoclay almost exclusively places into the not-extractable polyamide, in which high-temperature residual is close to the expected value of 9.4% computed assuming that all the organoclay locates inside PA6. The discrepancies are ascribable to uncertainty in the actual sample composition.

3.3. Analysis of the morphology on microscale

3.3.1. Scanning electron microscopy

Mixing two immiscible polymers in the melt state leads to a microstructure that depends on the fluid properties and flow history [28]. On the other hand, fillers of nanometric sizes influence the phase stability and morphology of polymer blends [29–31]. Since the micron-scale arrangement of the phases strongly affects the final macroscopic properties of multicomponent systems, investigations on the micron level were performed by means of scanning electron microscopy.

The SEM micrograph of the non-extracted organoclay-rich polyamide phase is shown in Fig. 4a. The sample, appeared not self-supporting at the end of the extraction process, consists of separated and highly elongated structures with irregular surfaces. Energy dispersive X-ray (EDX) analyses were performed upon one of these structures and the resulting spectrum is shown in Fig. 4b. Besides gold, associated with the coating metal sputtered upon the sample, the presence of the montmorillonite clearly emerges, as indicated by the peaks of its main constituents (oxygen, aluminium and silicon). The peak of the carbon mainly derives from the polymer chains, although some contribution may arise also from the organomodifier of Cloisite® 15A. The elongated organoclay-rich PA6 structures originate from the elongational components of the composite flow field experienced by the material during the extrusion. We argue that both the subsequent cooling at the die exit and the stiffness of the organoclay platelets into the PA6 phase prevent the relaxation of filled drops to a more thermodynamically stable spheroidal morphology. However, changes in microstructure are expected when the HDPE/PA6/clay extruded pellets are melted again. This is the case of the disks used for rheological investigations, which were obtained by melting and compressing the extruded

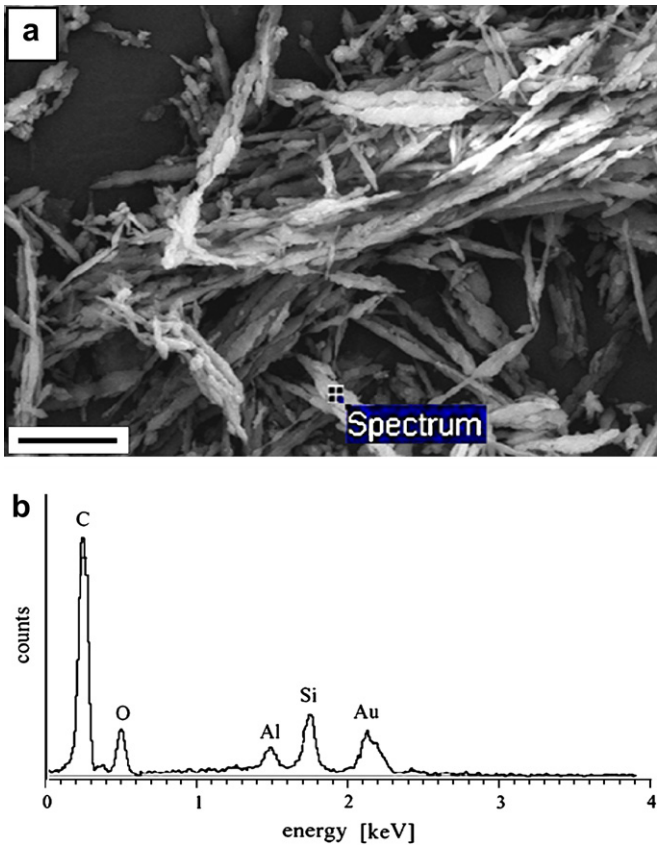

Fig. 4. (a) SEM micrographs of the non-extracted phase of the sample HDPE/PA6/clay. The scale bar represents 20 μm. (b) EDX spectrum evaluated in the selected zone of (a).

pellets between the parallel plates of the rheometer. Thus, SEM observations were carried out upon samples removed from the rheometer immediately before starting the rheological tests and the micrographs are shown in Fig. 5.

The blend HDPE/PA6 exhibits a globular microstructure, with the PA6 minor phase forming spherical drops suspended into the HDPE matrix (Fig. 5a). Due to the high interfacial tension, Γ, between the two immiscible polymers, the spherical morphology is the most thermodynamically favoured as it leads to the minimization of the specific interfacial area. In addition, the microvoids surrounding the PA6 droplets indicate that the interfacial adhesion is weak. Since the bulk properties of a polymer blend strongly depend on the quality of the interface, its modification using compatibilizing agents is generally required in order to get better final performances by promoting enhanced adhesion between the phases, low interfacial tension, and more uniform and finer dispersion of the minor phase. Typically, compatibilization is obtained by adding either a copolymer or a precursor that is able to promote the formation *in situ* of the interfacial agent [28]. In both cases, the compatibilization involves the interface region. Recently, a compatibilizing action related to the presence of organoclays in immiscible polymer blends has been reported in literature, although the physical mechanisms on the basis of the phenomenon are still not clear [7,23,32–34]. In order to verify a possible organoclay-related compatibilizing effect in the hybrid

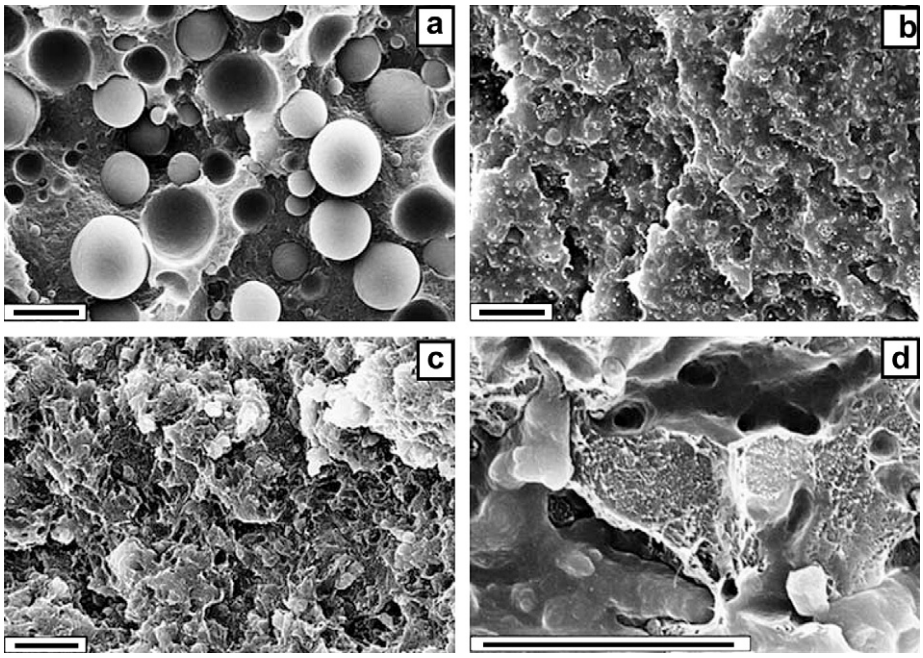

Fig. 5. SEM micrographs of various samples at the beginning of rheological tests: (a) HDPE/PA6, (b) HDPE/PA6/EAA, and (c,d) HDPE/PA6/clay. The scale bars represent 10 μm.

sample under investigation, a blend containing 5 phr of an ethylene–acrylic acid was used as reference material. EAA has been successfully used as a compatibilizer precursor in polyethylene/polyamide 6 blends: its presence causes an enhanced adhesion between the two phases, resulting in better mechanical properties and an improved morphological stability, i.e., a reduced coalescence rate on annealing. These phenomena have been explained with the formation of *in situ* copolymers EAA-*g*-PA6, acting as compatibilizers for the blend due to the partial solubility of EAA in the PE phase [35–38]. The microstructure of the blend HDPE/PA6/EAA is shown in Fig. 5b. The good interfacial adhesion ensured by EAA makes the PA6 droplets hardly observable, and the fracture surface appears smooth and uniform. However, it can be guessed that the dispersed phase keeps a spheroidal morphology, with drop sizes significantly reduced with respect to the uncompatibilized blend. The impact of the organoclay on the morphology of the sample HDPE/PA6/clay is shown in Fig. 5c. Although the absence of big spheroidal domains can be noticed, in contrast with the sample HDPE/PA6/EAA, the hybrid blend is characterized by a relevant roughness indicative of a poor interaction between the phases. This is confirmed by the analysis of the SEM micrograph at higher magnification shown in Fig. 5d, in which the hybrid sample appears phase separated, and highly distorted organoclay-rich PA6 big domains can be clearly recognized. Since neither an enhancement of the interfacial adhesion nor a clear reduction of the sizes of the minor phase emerges from the visual inspection of the micrographs of Fig. 5c and d, we conclude that the organoclay does not act as a classic compatibilizer like EAA, and it alters the microstructure of the hybrid blend under investigation through a mechanism which does not involve the enhancement of interfacial adhesion. We remark, however, that the organoclay stabilizes the morphology of the sample HDPE/PA6/clay, as indicated by the deformed shape of the filled minor phase shown in Fig. 5d.

3.3.2. Quantitative extraction experiments

Remarkably, as a consequence of the irregular shape of the inclusions, the polymer phases seem interpenetrated, suggesting that the elongated organoclay-rich PA6 domains shown in Fig. 4a, originally separated in the extruded pellets, could interconnect during the subsequent melting required for rheological investigations to form a co-continuous morphology. On this subject, however, SEM analysis alone does not provide complete information because of its two-dimensional feature. In order to check the degree of co-continuity, φ, of the hybrid blend, quantitative extraction experiments were performed as well by selectively removing the polyamide phase of the samples using formic acid. The results are summarized in Table 4 for the neat and filled blends. For the sample HDPE/PA6, we found $\varphi = 22.8\%$ that is a surprisingly high value considering that this blend has a droplet morphology (Fig. 5a). Solvent extraction experiments for the detection of co-continuity are affected by sample size due to the dissolution of the dispersed particles at the surface of the sample [39]. Testing samples with different sizes and performing an extrapolation procedure

Table 4
Results of quantitative extraction experiments

Sample	PA6 content[a] (wt%)	Clay content[a] (wt%)	Weight loss (wt%)	φ (%)
HDPE/PA6	25	–	5.7	22.8
HDPE/PA6/Clay	23.8	4.8	25.4	$\geq$87.3

[a] Nominal contents.

would be required to account for this effect, but for the purposes of our study we simply remark that the influence of sample size becomes more and more negligible as $\varphi \to 1$ [40]. The correct estimation of m_f for the sample HDPE/PA6/clay is difficult due to the loss of an unknown fraction of organoclay contained into the dissolving PA6. Thus, only an inferior limit is reported for the φ of the hybrid blend, representing the degree of co-continuity computed assuming that all the organoclay is lost during the extraction. Since such a scenario seems unlikely, and reminding the negligible sample size effect for samples with high degree of co-continuity, the value of $\varphi \geq 87.3\%$ clearly indicates that, if not fully co-continuous, polyamide in the nanocomposite blend is characterized by a very high degree of continuity.

Despite the low content of PA6, morphological analyses indicate that the nanocomposite blend can be approximately depicted as a continuous network of an organoclay-rich polyamide phase interspersed and poorly interacting with the host HDPE. Recently, several authors have observed the unexpected formation of co-continuous morphologies in polymer blends filled with organomodified clays [41–44]. Although the exact mechanisms on the basis of the phenomenon are not clear, a common feature characterizing all the systems is the selective placement of the filler inside only one of the polymer phases. Moreover, the authors generally claim the failure of the classical approaches employed to predict the development of co-continuous morphologies in unfilled polymer blends. In these simpler systems co-continuity occurs around the phase inversion point, where the distinction between the disperse and matrix phases vanishes. Several empiric relations [45,46] and theories [47] have been reported giving the volume fraction for phase inversion as a function of the ratio between the viscosities of the blend constituents. These relations, however, do not take into account any requirement as to the shape of the minor component necessary to obtain co-continuity. Full co-continuity may develop also at low volume fraction of either phase if the minor blend component consists of elongated structures. Willemse et al. derived an empirical relationship for co-continuity in unfilled polymer blends starting from simple geometrical requirements [48,49]. Depicting the continuous minor phase as an assembly of rod-like particles randomly oriented and at their maximum packing density, Φ_{max}, inside the major component, the following relationship can be written:

$$\frac{1}{\Phi_{max}} = 1.38 + 0.0376\left(\frac{L}{B}\right)^{1.4} \quad (1)$$

where L is the length and B is the diameter of the rods. The formation and stability of elongated structures in unfilled polymer blends require appropriate blending conditions. Moreover, the quick cooling of the material below the melt or glass temperature of one of the components is necessary at the end of the process in order to avoid the minor phase that retracts back to spheres or breaks up into smaller fragments driven by interfacial tension.

The filled polyamide phase of the sample HDPE/PA6/clay exhibits rod-like morphology in the extruded pellets (Fig. 4a). Thus, Eq. (1) can be used as a first approximation, although the hypothesis of random orientation of the organoclay-rich PA6 domains should not be verified on microscale in the system under investigation. An analysis of the SEM micrograph of Fig. 4a leads to $L/B \sim 20$. Introducing this value in Eq. (1) gives $\Phi_{max} \sim 25.8\%$. By assuming the additivity of the volumes of PA6 and organoclay, the volume fraction of the organoclay-rich polyamide phase in the sample HDPE/PA6/clay is $\Phi \sim 24.4\%$, making plausible that the elongated and separated domains shown in Fig. 4a may touch each other in the earlier stages of the melting of the pellets between the plates of the rheometer. Such a percolating structure may lead to a continuous network as a consequence of the merging of the inclusions in the contact points driven by the high interfacial tension between PA6, encapsulating the organoclay, and the HDPE suspending medium. Furthermore, quantitative extraction experiments indicate that the so-formed co-continuous microstructure persists in the melt state for ~300 s that is the typical time required to generate the disks for rheological analyses starting from the extruded pellets. We explain this experimental evidence by considering that the co-continuous morphology cannot evolve to a phase-separated morphology in the timescale of our experiments due to the organoclay framework, which would radically slow down the melt state dynamics of the percolating network as discussed in detail in the next paragraph.

3.4. Melt state behaviour – linear viscoelasticity

Rheology represents a suitable investigation tool to investigate the melt state behaviour on the basis of the complex morphology exhibited by the studied materials. In particular, linear viscoelastic measurements allow probing into the dynamics of the samples without affecting their microstructure. Performing oscillatory frequency scans in the linear regime is the simplest way to inspect the viscoelastic properties of a fluid. Such kind of test, however, strictly requires the stability of the melt state properties during time. Conversely, the studied hybrid blend may experience temporal evolutions due to changes occurring on both micro- and nanoscale arising from the morphological instability of the polymer phases [50] and alterations in the state of dispersion of the organoclay [51,52]. The neat HDPE itself exhibits the growth of both moduli during time probably due to thermal-promoted changes in its molecular architecture. Monitoring the temporal evolutions of the G' and G'' allows investigating the timescales of these ageing phenomena. The elastic moduli at 240 °C of the sample HDPE/PA6/clay at various frequencies are shown as a function of time in Fig. 6. The sample's elasticity remarkably increases during time, the growth rate being more pronounced at low frequencies. A similar trend was detected also for the viscous modulus, but the ageing effects on G'' appears much less prominent. A suitable way to evade the temporal dynamics of the samples and capture their mere frequency-dependent viscoelastic behaviour is to use multiwave rheology. The

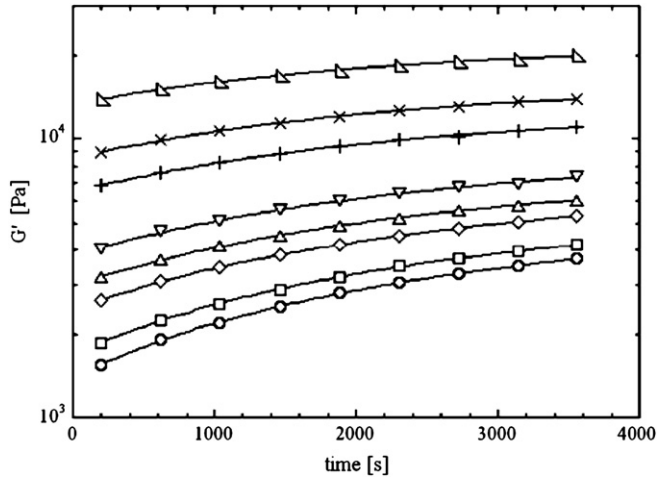

Fig. 6. Evolutions during time of the elastic modulus at 240 °C for the sample HDPE/PA6/clay at $\omega = 0.1$ (○), 0.2 (□), 0.6 (◇), 1 (△), 2 (▽), 6 (+), 10 (×), and 20 (◺) rad/s. Solid lines are guides for the eye.

advantage arises from the short duration of multiwave tests, corresponding to the time required to complete one cycle of strain at the fundamental frequency. Setting $\omega_f = 0.1$ rad/s we contained the duration of a multiwave test within ~150 s, making negligible the temporal evolutions of the viscoelastic properties. The linear viscoelastic moduli for different samples, extended up to $\omega = 10^2$ rad/s by means of quick frequency scans, are shown in Fig. 7a and b. Due to the short duration of tests, we remark that the data reflect the structure of the samples shown in Fig. 5. Both the neat blend constituents show a liquid-like behaviour, with G'' significantly higher than G' in the whole range of frequencies investigated. The sample HDPE/PA6 exhibits the peculiar behaviour of an immiscible polymer blend [53]: its moduli, higher than those of the predominant HDPE phase, approach those of the matrix at high frequencies, while a shoulder characterizes G' at low frequencies as a consequence of the interface contribution to the blend elasticity. Once the frequency-dependent storage modulus of the blend is available, the emulsion model of Palierne [54,55] allows estimating the ratio between the volume-average drop radius, R_v, and the interfacial tension Γ, provided that the polydispersity index, i.e. the ratio between the volume- and the number-average drop radii (R_n), does not exceed 2.3 [56]. The analysis of the SEM micrographs of the blend HDPE/PA6, performed by correcting the PA6 drop sizes according to Wu's approach [57], leads to $R_v = 4.2$ μm and $R_v/R_n = 1.41$, enabling the use of Palierne's model under the assumption that R_v is the representative drop size of sample. The solid line of Fig. 7a represents the fit of Palierne's model to the experimental G' data of blend obtained using Γ as the fitting parameter. The computed value of the interfacial tension is $\Gamma = 17.2$ mN/m, which is in good agreement with the values reported in the literature for HDPE/PA6 blends [58,59]. Although confined within the PA6 minor phase, the organoclay has a drastic effect on the viscoelasticity of the sample HDPE/PA6/clay. Blends with a co-continuous morphology usually exhibit a power law-like relaxation of the

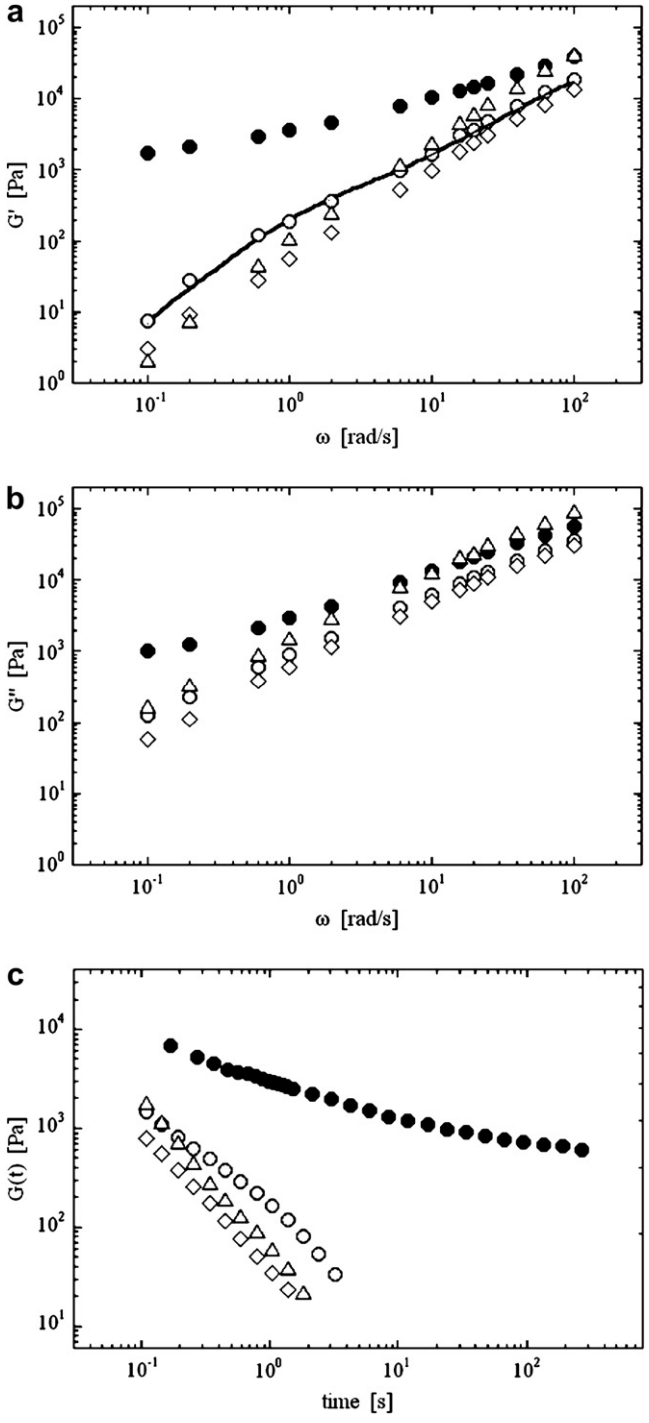

Fig. 7. (a) Elastic, (b) viscous and (c) stress relaxation moduli of HDPE (◇), PA6 (△), HDPE/PA6 (○), and HDPE/PA6/clay (●). Solid line in (a) represents the fit of Palierne's model to the experimental G' data of the blend HDPE/PA6 obtained using the interfacial tension Γ as the fitting parameter.

elastic modulus at low frequencies. This is ascribed to the presence of domains with different characteristic length scales, resulting in a continuous relaxation time spectrum [60,61]. The outstanding increase of both moduli of the hybrid blend, however, cannot be merely described in terms of morphological factors, and the striking effect of the organoclay has to be taken into account. The hybrid blend shows many peculiar

features of a one-phase polymer based nanocomposite, such as the emerging of a striking elasticity and a weak dependence of both moduli on ω at low frequencies [62]. The faster hybrid dynamics, however, approach those of the HDPE neat matrix. Thus, the viscoelastic behaviour of the sample HDPE/PA6/clay can be roughly explained assuming the existence of at least two distinct populations of dynamical species: the major polyethylene phase, unaffected by the filler and governing the hybrid rheology at short times, and a slower species, responsible for the long timescale behaviour, involving the filled PA6. According to this simplified physical picture, the low-frequency behaviour of the hybrid blend reduces to that of a one-phase PA6-based nanocomposite. In order to probe into the dynamics of this species at longer times, stress relaxation experiments were performed. The duration of tests was contained within $\sim$300 s in order to minimize the ageing effects previously discussed. The stress relaxation moduli, $G(t)$, of the neat blend constituents, the unfilled blend, and the hybrid blend are compared in Fig. 7c. Besides a dramatic slackening of relaxation processes, the sample HDPE/PA6/clay is characterized by the absence of terminal relaxation within the experimental time window. The existence of a three-dimensional network is generally proposed in order to explain the solid-like feature generally characterizing the slower dynamics of polymer nanocomposites based on a single polymer. Such a network may result from either direct interaction between particles [63,64] or polymer–filler networking processes [65,66]. Discriminating between the two mechanisms would require the knowledge of the complex chemical/physical interactions between the polyamide chains and the filler, which is beyond the scope of this study. Looking at the deformed shape kept for long time in the melt state by the organoclay-rich polyamide phase (Fig. 5d), we can speculate that the slackening of dynamics does not concern the filler only, but the hindering of the mobility of a large fraction of polyamide chains should also be considered. Whatever the nature of the space-filling network be, however, rheological analyses elucidate the timescales characterizing the melt state behaviour of the filled minor phase, which is unable to relax at times shorter than $\sim$300 s. This means that, once formed, the co-continuous morphology in the sample HDPE/PA6/clay is greatly stabilized by the organoclay, confirming our previous hypotheses about the relevance of the filler in preserving the co-continuous morphology. Finally, we emphasize that the characteristic times of most of the transforming processes in the polymer industry are much shorter than the timescales for the macroscopic relaxation of the sample HDPE/PA6/clay. This implies that, in addition to the processing parameters, the organoclay may represent an efficient material parameter for the tailoring of the final blend properties.

3.5. Solid state behaviour – mechanical properties

The specimens for tensile test were cut from plates obtained by compression molding of the extruded pellets. Due to the specificity of the thermomechanical history at which the compression-molded samples were subjected, quantitative extraction experiments were performed in order to check the co-continuity of the hybrid specimens and a range of φ comparable with that of the disks used for rheological measurements was found.

Table 5
Young's moduli (E), tensile strengths (TS) and elongations at break (EB) for various samples

Samples	E (MPa)	TS (MPa)	EB (%)
HDPE	776	23.5	950
PA	903	36	230
HDPE/PA	742	21	110
HDPE/PA/EAA	840	28	180
HDPE/PA6/Clay	1150	32	95

The average values of Young's modulus, E, tensile strength, TS, and elongation at break, EB, are summarized in Table 5. The weak interfacial adhesion between the polymer phases rules the tensile properties of the blend HDPE/PA6, which result lower than those of the neat polymers due to the poor stress transfer across the interface and the non-homogeneity of the sample on microscale. As previously discussed, EAA promotes the improvement of the interfacial properties of the compatibilized blend. As a consequence, the mechanical properties of the sample HDPE/PA6/EAA increase with respect to the neat blend, although the elongation at break remains lower than those of the pure components. A remarkable enhancement of the elastic modulus characterizes the blend HDPE/PA6/clay in spite of the poor interfacial adhesion emerged from SEM analyses (Fig. 5c and d). We emphasize that such result stems from the co-continuous morphology of the hybrid blend, with both the HDPE and the filled PA6 contributing to mechanical strength without stress being transferred across the interface [67,68]. On the other hand, the probable loss of ductility of the organoclay-rich polyamide phase and the poor interfacial adhesion emerged from the microstructural analyses (Fig. 5c and d) may explain the low elongation at break exhibited by the sample HDPE/PA6/clay.

4. Conclusions

In the present study, the effect of an organomodified clay on the morphology and properties of an HDPE/PA6 blend was investigated. The filler locates exclusively inside the more hydrophilic polyamide phase during the melt compounding. As a consequence, a complex microstructure forms with organoclay-rich PA6 separated and elongated domains interspersed with the host HDPE. The morphology of the extruded sample, however, evolves to a co-continuous morphology when the extrudate is melted again. The organoclay does not promote the enhancement of the interface adhesion and the phases remain separated. Rheological tests show that the co-continuous microstructure confers to the nanocomposite blend many peculiar features of single-phase polymer-layered silicate nanocomposites. The analysis of the melt state dynamics suggest the existence of two distinct populations of dynamical species: the major polyethylene phase, unaffected by the filler and

governing the hybrid rheology at short times, and a slower species, responsible for the long timescale behaviour, involving the filled PA6. The dramatically slackened dynamics of the latter species greatly stabilizes the morphology of the hybrid blend in the melt state. Despite the weak interfacial adhesion, the co-continuous structure of the nanocomposite blend results in improved mechanical properties because both phases can contribute the mechanical strength without stress being transferred across the interface.

Acknowledgements

The authors thank Prof. P.L. Magagnini from University of Pisa for X-ray spectra.

References

[1] Holsti-Mettinen RM, Perttila KP, Seppälä JV, Heino MT. J Appl Polym Sci 1995;58:1551.
[2] Srinivas LT, Kale DD. J Polym Mater 1997;14:7.
[3] Jarus D, Hiltner A, Baer E. Polymer 2002;43:2401.
[4] Usuki A, Kojima Y, Kawasumi M, Okada A, Fukushima Y, Kurauchi T, et al. J Mater Res 1993;8:1179.
[5] Giannellis EP. Appl Organomet Chem 1999;12(10–11):675.
[6] Zanetti M, Lomakin S, Camino G. Macromol Mater Eng 2000;279(1):1.
[7] Schmidt D, Shah D, Giannelis EP. Curr Opin Solid State Mater Sci 2002;6(3):205.
[8] Ray SS, Okamoto M. Prog Polym Sci 2003;28(11):1539.
[9] Ahmadi SJ, Huang YD, Li W. J Mater Sci 2004;39(6):1919.
[10] Jordan J, Jacob KI, Tannenbaum R, Sharaf MA, Jasiuk I. Mater Sci Eng A Struct 2005;393(1–2):1.
[11] Wang S, Hu Y, Wang Z, Yong T, Chen Z, Fan W. Polym Degrad Stab 2003;80:157.
[12] Park JH, Jana SC. Polymer 2003;41:3887.
[13] Mehrabzadeh M, Kamal MR. Polym Eng Sci 2004;44(6):1152.
[14] Chow WS, Mohd Ishak ZA, Karger-Kocsis J. Macromol Mater Eng 2005;290:122.
[15] Lee MH, Dan CH, Kim JH, Cha J, Kim S, Hwang Y, et al. Polymer 2006;47:4359.
[16] Li J, Ma PL, Favis DB. Macromolecules 2002;35:2005.
[17] Lyngaae-Jorgensen J, Utracki LA. Polymer 2003;44:1661.
[18] Dennis HR, Hunter DL, Chang D, Kim S, White JL, Cho JW, et al. Polymer 2001;42:9513.
[19] Torre L, Lelli G, Kenny JM. J Appl Polym Sci 2006;100:4957.
[20] Saha RK, Paul DR. Polymer 2006;47:4075.
[21] Chow WS, Mohd Ishak ZA, Karger-Kocsis J, Apostolov AA, Ishiaku US. Polymer 2003;44:7427.
[22] Chow WS, Ishiaku US, Mohd Ishak ZA, Karger-Kocsis J, Apostolov AA. J Appl Polym Sci 2004;91:175.
[23] Feng M, Gong F, Zhao C, Chen G, Zhang S, Yang M. Polym Int 2004;53:1529.
[24] Kohan MI, editor. Nylon plastic handbook. New York: Hanser/Gardner Publications, Inc.; 1997. p. 69–137.
[25] Liu L, Qi Z, Zhu X. J Appl Polym Sci 1999;71:1133.
[26] Lincoln DM, Vaia RA, Wang Z-G, Hsiao BS, Krishnamoorti R. Polymer 2001;42:9975.
[27] Bureau MN, Denault J, Cole KC, Enright GD. Polym Eng Sci 2002;42(9):1897.
[28] Utracki LA, editor. Commercial polymer blends. London: Chapman and Hall; 1998. p. 99–104.
[29] Karim A, Douglas JF, Nisato G, Liu DW, Amis EJ. Macromolecules 1999;32:5917.
[30] Lipatov YS, Nesterov AE, Ignatova TD, Nesterov DA. Polymer 2002;43:578.
[31] Vermant J, Cioccolo G, Golapan Nair K, Moldenaers P. Rheol Acta 2004;43:529.
[32] Voulgaris D, Petridis D. Polymer 2002;43(8):2213.
[33] Gelfer MY, Song HH, Liu L, Hsiao BS, Chu B, Rafailovich M, et al. J Polym Sci Part B Polym Phys 2003;41(1):44.
[34] Wang Y, Zhang Q, Fu Q. Macromol Rapid Commun 2003;24:231.
[35] Filippi S, Chiono V, Polacco G, Paci M, Minkova L, Magagnini PL. Macromol Chem Phys 2002;203:1512.
[36] Valenza A, Visco AM, Acierno D. Polym Test 2002;21(1):101.
[37] La Mantia FP, Scaffaro R, Valenza A, Marchetti A, Filippi S. Macromol Symp 2003;198:173.
[38] Minkova L, Yordanov Hr, Filippi S, Grizzuti N. Polymer 2003;44(26):7925.
[39] Galloway JA, Macosko CW. Polym Eng Sci 2004;44(4):714.
[40] Galloway JA, Koester KJ, Paasch BJ, Macosko CW. Polymer 2004;45:423.
[41] Ly Y, Shimizu H. Polymer 2004;45:7381.
[42] Ly Y, Shimizu H. Macromol Rapid Commun 2005;26:710.
[43] Wu D, Zhou C, Zhang M. J Appl Polym Sci 2006;1021:3628.
[44] Ray SS, Bandyopadhyay J, Bousmina M. Macromol Mater Eng 2007;292:729.
[45] Miles IS, Zurek A. Polym Eng Sci 1988;28:796.
[46] Ho RM, Wu CH, Su AC. Polym Eng Sci 1990;30:511.
[47] Utracki LA. Polym Mater Sci Eng 1991;65:50.
[48] Willemse RC, Posthuma de Boer A, van Dam J, Gotsis AD. Polymer 1999;40:827.
[49] Willemse RC, Posthuma de Boer A, van Dam J, Gotsis AD. Polymer 1998;39(24):5879.
[50] Filippone G, Netti PA, Acierno D. Polymer 2007;48(2):564.
[51] Reichert P, Hoffman B, Bock T, Thomann R, Mulhaupt R, Friedrich C. Macromol Rapid Commun 2001;22:519.
[52] Galgali G, Ramesh C, Lele A. Macromolecules 2001;34(4):852.
[53] Tucker III CL, Moldenaers P. Annu Rev Fluid Mech 2002;34:177.
[54] Palierne JF. Rheol Acta 1991;29:204.
[55] Palierne JF. Rheol Acta 1990;30:497.
[56] Graebling D, Muller R, Palierne JF. Macromolecules 1993;26:320.
[57] Wu S. Polymer 1985;26:1856.
[58] Liang H, Xu R, Favis BD, Shreiber HP. J Polym Sci Part B Polym Phys 2000;38:2096.
[59] Chapleau N, Favis BD, Carreau PJ. J Polym Sci Part B Polym Phys 1988;36:1947.
[60] Weis C, Leukel J, Borkenstein K, Maier D, Gronski W, Friedrich C, et al. Polym Bull 1998;40:235.
[61] Vinckier I, Laun HM. Rheol Acta 1999;38:274.
[62] Yurekli K, Krishnamoorti R. Curr Opin Colloid Interface Sci 2001;6(5):464.
[63] Mitchell CA, Krishnamoorti R. J Polym Sci Part B Polym Phys 2002;40:1434.
[64] Ren J, Krishnamoorti R. Macromolecules 2003;36:4443.
[65] Zhang Q, Archer LA. Langmuir 2002;18:10435.
[66] Sarvestani AS, Picu CR. Rheol Acta 2005;45:132.
[67] Fayt R, Jerome R, Teyssie P. J Polym Sci Part B Polym Phys 1989;27:775.
[68] Veenstra H, Verkooijen PCJ, van Lent BJJ, van Dam J, Posthuma de Boer A, Nijhof AHJ. Polymer 2000;41:1817.